STRUCTURAL CONTROL AND HEALTH MONITORING
Struct. Control Health Monit. 2013; **00**:1–**??**
Published online in Wiley InterScience (www.interscience.wiley.com). DOI: 10.1002/stc

AN OPTIMISED TUNED MASS DAMPER/HARVESTER DEVICE

A. Gonzalez-Buelga[1]*, L.R. Clare[1], A. Cammarano[1], S.A. Neild[1], S. G. Burrow [1]and D.J. Inman[1]

[1] *Faculty of Engineering. University of Bristol, UK.*

SUMMARY

Much work has been conducted on vibration absorbers, such as tuned mass dampers, where significant energy is extracted from a structure. Traditionally this energy is dissipated through the devices as heat. In this paper the concept of recovering some of this energy electrically and reuse it for structural control or health monitoring is investigated. The energy dissipating damper of a TMD is replaced with a electromagnetic device in order to transform mechanical vibration into electrical energy. That gives the possibility of controlled damping force whilst generating useful electrical energy. Both analytical and experimental results from an adaptive and a semi-active tuned mass damper/harvester are presented. The obtained results suggest that sufficient energy might be harvested for the device to tune itself to optimize vibration suppression.

Received . . .

KEY WORDS: Vibration reduction, Semi active control, Variable damping, Energy Harvesting

1. INTRODUCTION

Vibration suppression has been a major research topic for over a century, since Frahm [1] presented the first tuned mass damper, TMD, in 1911. Passive devices were studied in depth by Den Hartog a few decades later [2]. **The effectiveness of passive devices in some scenarios is limited [3] and very sensitive to mistuning problems [4]**. Over the past fifty years a number of adaptive, semi-active and active control laws have been developed in order to improve the performance of the original passive TMD [5, 6, 7, 8, 9, 10]. Traditionally these control forces were dissipated through the devices as heat and thus energy dissipation is often associated with undesirable self-heating problems. Instead this energy can be converted into electricity by means of different mechanisms such electromagnetism, electrostatic generation or the use of piezoelectric materials. More recently with the development of energy harvesting technologies, see Inman [11], research into combining structural control and energy harvesting has emerged as a prominent and growing research area [12, 14, 13]. In [12] the concept of simultaneously reduce vibration and harvest energy is studied numerically following the fixed point methodology developed by Den Hartog. Both [13] and [14] present experimental results from vibration absorbers/harvesters. In [13] simulations of semi-active and active control circuits are presented while the experiments concentrate on passive matching. The work presented in [14] details the modelling of a nonlinear triphasic electromagnetic device and presents experimental results demonstrating TMD impedance matching. In [15], the ability of linear electromagnetic actuators to act as dampers is examined. The vibration energy was dissipated by four different passive electrical subsystems. The same idea, the dissipation

*Correspondence to: A.GonzalezBuelga@bristol.ac.uk

of vibrational energy electrically, was also studied in [16], as a way to overcome self-heating issues. Using vibrating energy as a source of power for wireless transducers in civil engineering applications using electromagnetic transducers was studied in [17, 18]. In [17] it is shown that it is possible to charge a small battery out of the vibration energy taken from the environment. The optimisation of the energy conversion is studied in [18], in this work the electromagnetic transducer is connected to a flexible structure. **In the vehicle suspension research community, the development of regenerative suspensions have been proposed, which has the potential to both harvest energy and reduce the vibration response, see detailed review in [19].**

The present work reports on the controller development, power conditioning and experimental testing of a Tuned Mass Damper/Harvester (TMD/H), based on an electromagnetic linear motor. This device is capable of generating in the order of mW of power from low frequency structural vibrations while performing structural control. The basic conversion consists of a linear voice coil motor connected to a resistance emulator consisting of rectification and variable impedance unit. The resistance emulator is a power conditioning system that presents a controllable resistive load to the voice coil. The output of the resistance emulator is DC and can be used to power other circuits or charge a battery.

The paper is structured as follows, the next section reports a numerical parametric study of the system formed by a host structure with a coupled TMD/H. It includes the linear modelling of the chosen conversion device, a voice coil motor. Section 3 presents the power conditioning unit: voltage rectification and resistance emulator. This is an electronic circuit capable of acting as a tunable damper while dissipating minimal power and maintaining a fixed voltage output, the ideal scenario to deliver the harvested power to a power bus or a rechargeable battery [20]. In the same section two low power controllers, one adaptive and the other semi-active, are presented. Both controllers are based on adjustable damping forces. Section 4 includes the experimental testing of the proposed scheme, obtained by performing real time dynamic substructuring (RTDS) testing [21]. RTDS allows testing components of a structure offering advantages in terms of cost and versatility while offering reliable results if a good control of the transfer system is developed [22]. The results obtained from the RTDS tests suggest the enough power is generated so the proposed TMD/H is self tunning and self powered.

2. HOST STRUCTURE AND TMD/H COUPLED SYSTEM

This section defines the problem being considered: the interaction between a host structure and a TMD/H device in terms of vibration absorption and power available to harvest. A schematic of the coupled system is shown in Figure 1. The host structure is defined by (M_p,C_p,K_p) and the TMD/harvester by (M_s,C_s,K_s,F_{EM}). Figure 1 shows two different possible external actions: force F_e and ground acceleration a_g.

The idea is to replace the traditional energy dissipating damper in the TMD (or at least part of it since it is impossible to avoid completely parasitic damping) with an electromagnetic device, providing energy conversion and damping regulation capabilities. In our study the objective is to reduce displacement of the host structure and to transform part of the vibrational energy absorbed into usable energy so: (i) our device can be self-powered if control laws are needed and (ii) sensor nodes can be powered for health monitoring purposes.

The equations of motion for the host structure coupled with a TMD/Harvester, when subjected to external forcing f_e, can be written as:

$$\begin{aligned} M_p\ddot{x}_p + C_p\dot{x}_p + K_p x_p - C_s\dot{x}_s - K_s x_s - F_{EM} &= f_e \\ M_s(\ddot{x}_p + \ddot{x}_s) + C_s\dot{x}_s + K_s x_s + F_{EM} &= 0 \end{aligned} \tag{1}$$

where M,C,K, represent mass, stiffness and damping, respectively. Subscript p relates to the host structure while subscript s relates to the TMD/H. x_p represents the displacement of the host structure relative to ground and x_s represents the displacement of the TMD/H relative to the host structure,

DOI: 10.1002/stc

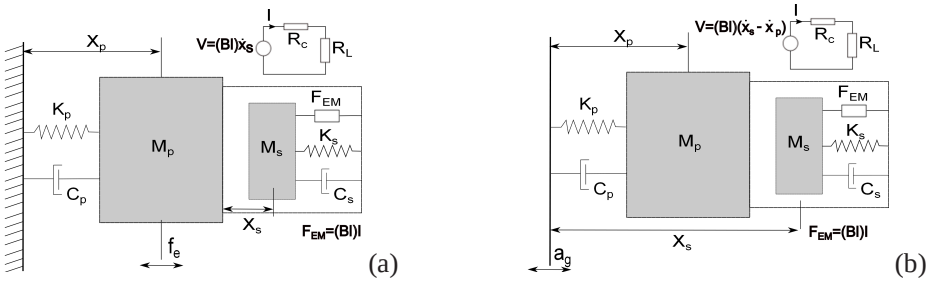

Figure 1. Host structure and TMD/H coupled system showing external forcing (a) and base excitation (b), which will be considered in turn.

as shown Figure 1 (a). F_{EM} represents the force reflected back by the electromagnetic device into the mechanical domain.

Here we consider an electromagnetic device, a moving magnet DC voice coil linear actuator manufactured by h2wtech, whose characteristics are listed in Table I. The device, model NCM30-25-090-2LB, was chosen for its nearly ideal mechanical properties over a specific range of displacement, that yielded an acceptably high output voltage, together with its electromagnetic coupling constant that was almost perfectly constant over the displacement range. The device is governed by the Lorentz Force Equation $F_{EM} = (Bl)I$ where Bl is the Flux density or electromagnetic coupling constant and I is the current. Since the permanent magnet flux density field is fixed, the direction of electromagnetic force F_{EM} depends on the polarity of current and vice versa. The mass in the system is the moving magnet plus a lumped mass mounted onto the shaft, the stiffness is given by two springs acting in parallel with the shaft. Figure 2 shows the tested arrangement, which is described in detail in section 4. When the magnet is excited, a voltage is generated as the magnet moves through the magnetic field. This voltage V is proportional to the velocity of the magnet, $V = (Bl)\dot{x}_s$. With the coil open-circuit, damping is due to internal losses such as eddy currents, mounting bearings or magnetic hysteresis. Electrical damping results when a circuit is completed between the ends of the coil, and is the means by which mechanical energy is converted into electrical energy.

Figure 2. Picture of the tested TMD/H

Mechanical

M_s	K_s	C_s
2.34kg	1200 N/m	21 N/(m/s)

Electrical

Bl	R_c
11.34 N/A	2.96 Ω

Table I. TMD/H parameters.

The force reflected back into the mechanical domain, taking into account Lorentz equation and velocity-voltage relationship, can be written as:

$$F_{EM} = \frac{(Bl)^2}{(R_c + R_L)}\dot{x}_s \tag{2}$$

where R_c and (Bl) are the internal coil resistance and electromagnetic coupling respectively. R_L is an optimal resistive load connected across the motor terminals. See Figure 1.

Substituting Equation (2) into Equation (1) and taking the Laplace transform, expressed in terms of $s = i\omega$, where $i = \sqrt{-1}$, we obtain

DOI: 10.1002/stc

$$\begin{aligned}\left(K_p - \omega^2 M_p + i\omega C_p\right) X_p - \left[K_s + i\omega\left(C_s + \frac{(Bl)^2}{(R_c + R_L)}\right)\right] X_s = F_e \\ -\omega^2 M_s\, X_p + \left[K_s - \omega^2 M_s + i\omega\left(C_s + \frac{(Bl)^2}{(R_c + R_L)}\right)\right] X_s = 0\end{aligned} \tag{3}$$

where X_s, X_p and F_e are the Laplace transforms of x_s, x_p and f_e respectively. We define the following parameters, $\mu = \dfrac{M_s}{M_p}$ is the mass ratio TMD/H to host structure, $\beta = \dfrac{\omega_s}{\omega_p}$ is the frequency ratio TMD/H to host structure and $r = \dfrac{\omega}{\omega_p}$ is the frequency ratio host structure to excitation frequency, using these we obtain the following equations:

$$\begin{aligned}\left(1 - r^2 - 2i\zeta_p r\right) x_p - \left(\mu\beta^2 + 2i\mu\zeta_T\beta\right) x_s = \frac{F_o}{M_p\omega_p} \\ -r^2 x_p + \left(\beta^2 - r^2 + 2i\mu\zeta_T\beta\right) x_s = 0\end{aligned} \tag{4}$$

where ζ_T is the total damping ratio presented to the host structure by the TMD/H, ζ_p is the host structure damping ratio. Noting that the total damping of the TMD/H $C_T = 2\omega_s M_s \zeta_T$ is a combination of mechanical and electrical terms, we obtain:

$$C_T = C_s + C_e \text{ where } C_e = \frac{(Bl)^2}{(R_c + R_L)} \tag{5}$$

Hence, the average power available to harvest can be calculated by considering the power dissipated in the resistive load R_L,

$$P_{avg} = \frac{1}{T}\int_0^T I^2 R_L dt = \frac{1}{T}\int_0^T \frac{(Bl)^2 \dot{x}_s^2}{(R_c + R_L)^2} R_L dt \tag{6}$$

2.1. Parametric study

The aim of this section is to show the strong coupling between the host structure and the TMD/H both in terms of vibration absorption and power. The system defined by Equation (4) has been studied in depth for passive systems [2, 6]. In our study the optimal parameters β and ζ_T are calculated for a given μ, with the objective being the reduction of the displacement of the host structure.

Our parametric study considers passive systems as well and starts by using the formulas presented by Den Hartog [2] for optimal vibration absorption, $\beta = 1/(1+\mu)$ and $\zeta_T = \sqrt{3\mu/(8(1+\mu))}$. **As a starting point for analysis, the optimal damping C_T is assumed to be equally divided between electrical and mechanical for simplicity. Note the effect of modifying this ratio is discussed later in Figure 4.** It is important to note that to be able to work in optimal conditions and harvest power simultaneously the optimal damping C_T must be larger than the mechanical one C_s. In the case of a TMD/H with high parasitic damping C_s, this results in the need to work with higher mass ratios μ.

Figure 3 (a) shows a simulation for $\mu = 0.05$ depicting displacement of the host structure and TMD/H. The other subfigures are obtained by varying μ, via M_s, while keeping constant the rest of the parameters. It can be seen that the higher the mass ratio, the more the displacement of the host structure is reduced. The rate of this reduction tends to lessen as μ increases, besides large mass ratios are undesirable for structural reasons. The peak value of power available to harvest reduces as we increase the mass ratio although we note an improvement in bandwidth at higher values of μ. Also the increase in power available to harvest as μ decreases is due to an increase in the relative displacement of the TMD/H, which will necessitate a larger device. This reveals a challenge, an optimal absorber is not an optimal harvester. Different optimal values for μ can be found depending

DOI: 10.1002/stc

on the quantity to optimise: vibration absorption, harvesting or a combination of the two, taking into account space and stroke limitations.

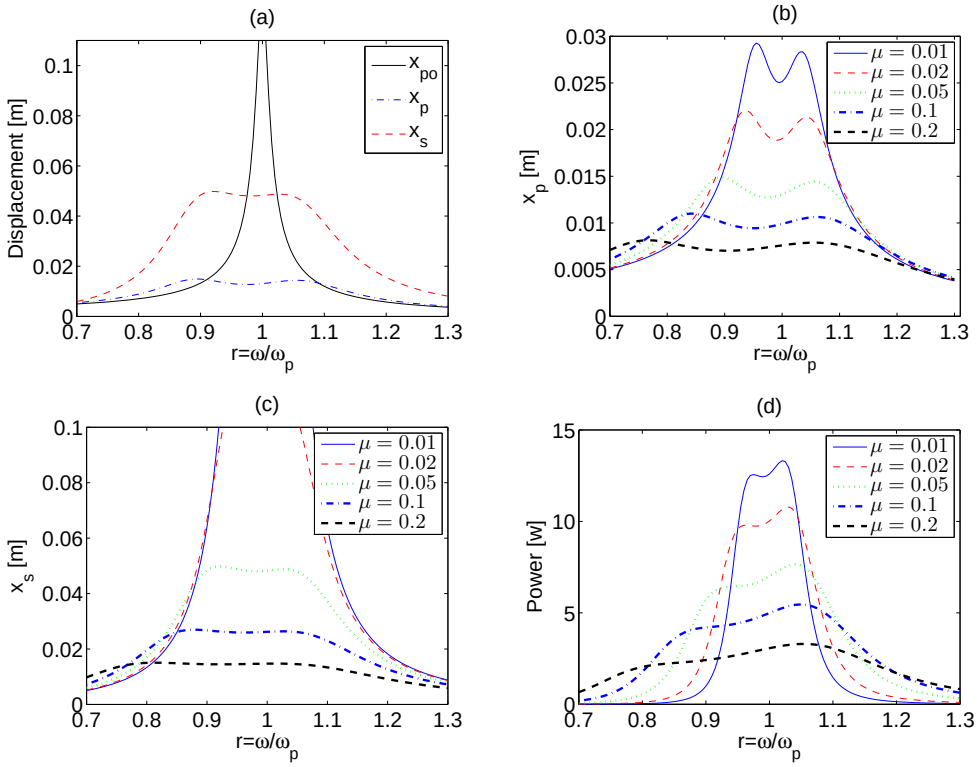

Figure 3. (a) Host structure displacement before x_{po} and after x_p TMD/H coupling with $\mu = 0.05$, x_s relative displacement of the TMD/H. (b) Host structure displacement evolution for different μ; (c) TMD/H relative displacement and (d) Power available to Harvest for different μ

Figure 4 shows the evolution of the power available to harvest for different electrical to mechanical damping ratios, $q = C_e/C_s$, for a fixed C_s. It can be seen that the ratio q at which the power available to harvest is maximum varies depending on μ and r. Recent studies on a pure harvester, where it was assumed there was not interaction between the host structure and the harvester, showed that the electrical damping has to be equal to the mechanical damping for maximum harvestable energy, i.e. $q = 1$, at resonance $\omega = \omega_s$, [23, 24]. In Figure 4(a), where $\mu = 0.01$, the optimal q at resonance is approximately $q = 5$, for higher values of μ, q will increase accordingly, see figure 4(b). This shows the importance of considering both host structure and harvester, when μ is of this order, even in the case when vibration absorption is not considered as part of the optimization procedure.

Figures 3 and 4 show results from a system were β take the value suggested by Den Hartog, in order to minimise the displacement of the host structure. Figure 5 shows the evolution of the power available to harvest for different values of β, given a fixed value for μ. The optimal β depends on the excitation frequency, if $r < 1$ then the optimal β is greater than unity and vice versa. For small values of μ the distance between the two optimal values is minimal and $\beta^- \approx \beta^+ \approx 1$, where β^- is the optimal value if $r < 1$ and β^+ is the optimal value if $r > 1$. For higher values of μ this distance increases.

In this section passive devices have been considered. Given the strong coupling between the host structure and the TMD/H, the whole system must be included in the optimisation problem. However at the limit case $\mu \to 0$ is approached, host structure and TMD/H decouple and cease to influence each other. From the harvesting point of view, both R_c and C_s have to be as low as possible, so

DOI: 10.1002/stc

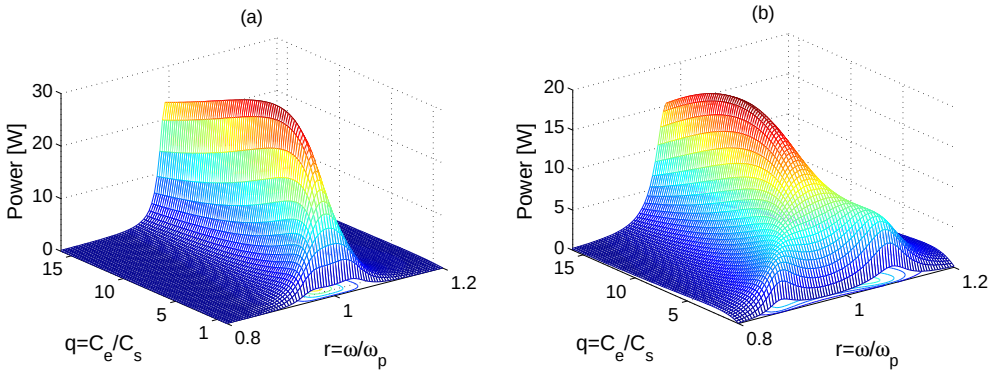

Figure 4. Power available to harvest versus frequency ratio ω/ω_p and damping ratio C_e/C_s. Both dissipative damping ζ_s and frequency ratio β are fixed at 5% and $\beta = \dfrac{1}{1+\mu}$ respectively. (a) $\mu = 0.01$ and (b) $\mu = 0.05$.

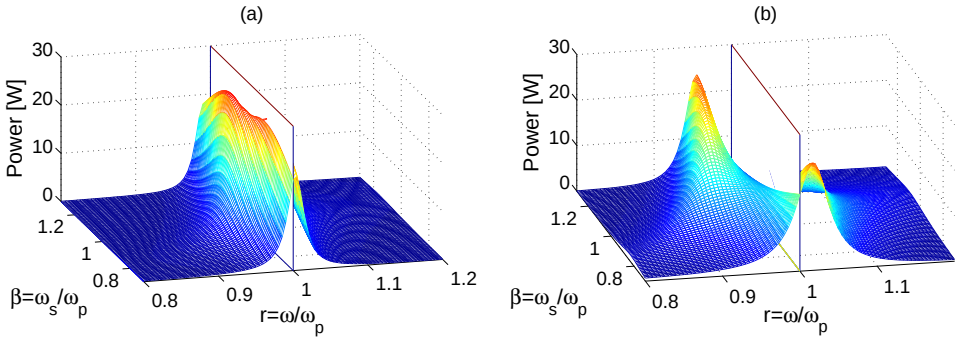

Figure 5. Power available to harvest versus frequency ratios $r = \omega/\omega_p$ and $\beta = \omega_s/\omega_p$. (a) $\mu = 0.01$ and (b) $\mu = 0.05$.

power available to harvest is maximum. Since vibration absorption does not distinguish between electrical and mechanical damping, these values are not critical, as long they do not exceed the optimal total values.

3. IMPLEMENTATION AND CONTROL

The simultaneous retuning of the TMD/H and recovery of the electrical power has been made possible by using a resistance emulator. This emulator is an electronic circuit that mimics the resistive load R_L in Equation (2). By using an emulator we are able to harvest energy and acquire the capability of changing R_L in real time hence performing control. Two low-power-consumption control laws were developed to improve the performance of a TMD in terms of displacement of the host structure. These control laws are based on controllable damping forces and were implemented via the resistance emulator. We now discuss both the emulator and control laws.

3.1. Resistance emulation and power conditioning

The resistance emulator is based on a rectifier followed by a switched-mode flyback converter, which when operating in discontinuous mode, has the property of emulating a resistance at its input terminals. When the electronic circuit shown in Figure 6 (a) is connected to the TMD/H, it $sees$ a resistive load R_L connected across its terminals. The resistance emulator allows changes of

DOI: 10.1002/stc

resistance value, the changes can be made to occur in milliseconds, allowing the damping to vary dynamically. Although the converter emulates a resistance, the power is not simply dissipated as heat as with a passive resistance, but most $(85\% - 90\%)$ is transferred to the output, a rechargeable battery, where it is available to supply the control circuit itself and a wireless conditioning-monitoring system [25]. **This principle was first proposed by [26, 27, 28], using a flyback converter, discontinuous conduction and a buck-boost converter respectively, to optimise energy conversion from piezoelectric materials.**

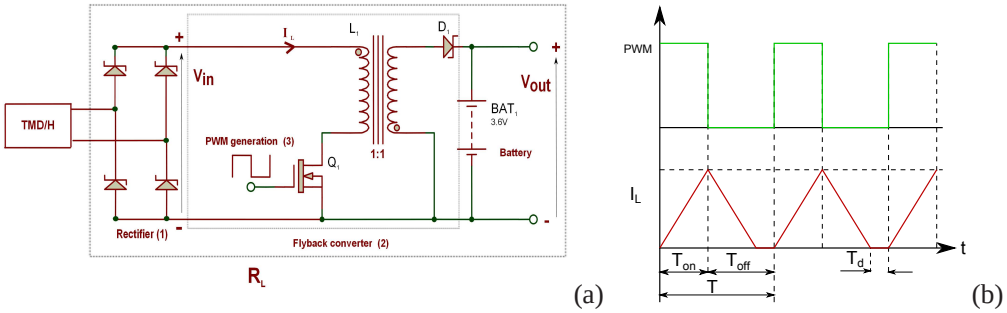

Figure 6. (a) Resistance emulator simplified structure: rectification + PWM generation + flyback converter. (b) Flyback converter waveforms in discontinuous mode. i.e $T_d > 0$.

Figure 6 (a) shows the basic configuration or the resistance emulator and (b) the operating waveforms with discontinuous inductor current, i.e $T_d > 0$. By considering the geometry of the inductor current during time T_{on}, the effective input resistance, R_L is given by, [25]:

$$R_L = \frac{2L_1}{D^2 T} \tag{7}$$

where L_1 is the value of the inductor, D is the pulse width modulation (PWM) duty-cycle, $D = T_{on}/(T_{on} + T_{off})$ and T is the PWM waveform period. In this case the frequency is fixed and therefore T is constant as is L_1, so the resistance is controlled by varying the duty-cycle. The above equation holds as long as the inductor current is discontinuous, $T_d > 0$, and a value of inductance is chosen to ensure this is the case using the equation [25]:

$$L_{crit} = \frac{(V_{in}V_{out})^2 T}{2P(V_{out} + V_{in})^2} \tag{8}$$

where P is the output power.

Figure 7 shows the complete circuit of the experimentally tested resistance emulator. As it can be seen in Figure 7 (c) comparator U2:A together with Q6, form a relaxation oscillator generating a sawtooth waveform at 25 kHz. This signal is fed to comparator U2:B, where it is compared to the duty-cycle control voltage obtained from a control law. The output of U2:B drives the gate of MOSFET Q6, see Figure 7 (b), switching it on and off as in the flyback converter shown in Figure 6 (b). The output is shunt regulated by a rechargeable battery at a suitable voltage. The value of the resistance R_L is controlled by the duty-cycle control voltage, a plot of resistance R_L against duty cycle control voltage obtained experimentally, is shown in Figure 7 (d).

When operating at relatively low power levels, as is always the case in energy harvesting, the following steps are taken to reduce the power overhead of the converter:

- using micro power comparators.
- operating at the relatively low switching frequency of 25KHz (as compared to $100kHz$ as used in normal practice).

DOI: 10.1002/stc

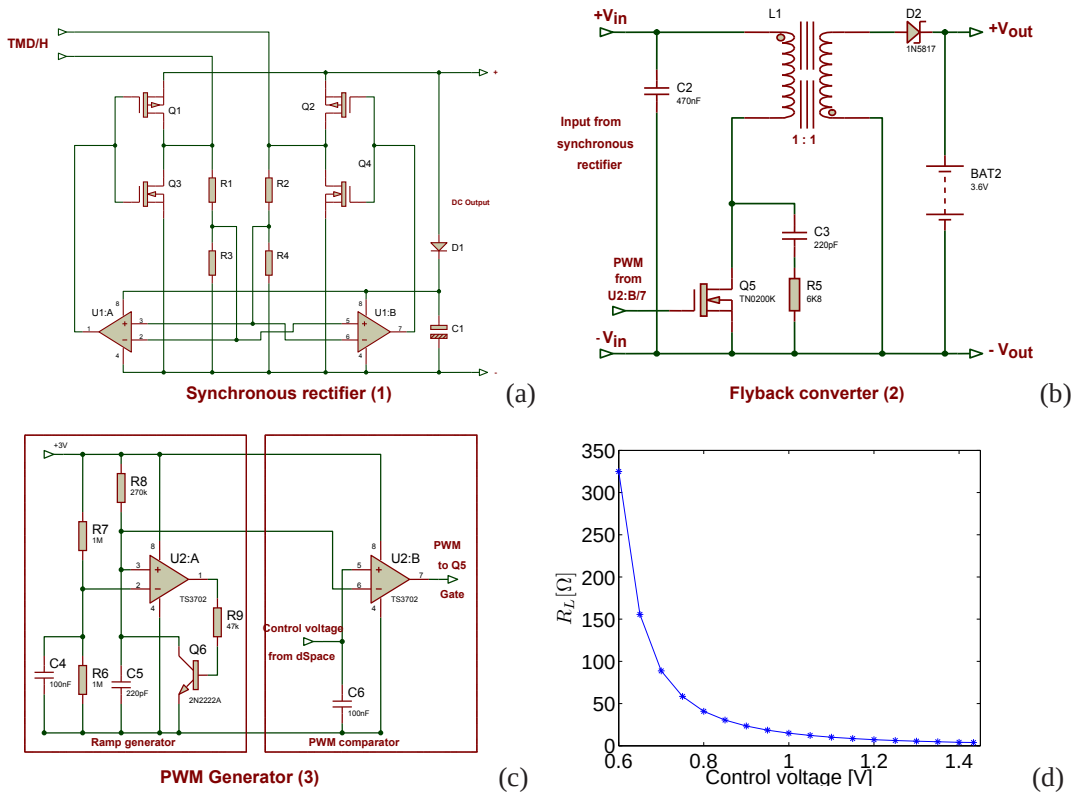

Figure 7. Schematic of the complete resistance emulator, (a) Synchronous rectification, (b) Complete flyback conveter, (c) PWM generation (d) experimental graph: duty cycle voltage versus resistive load presented to the harvester R_L

- operating the inductor at a very low flux density.

As the harvester generates an alternating voltage and the flyback converter is a direct current device, it must be preceded by a full wave rectifier. Because the voltage it is of a low value, less than 5 volts, the voltage drop of around 0.8 V incurred when using a diode bridge rectifier was deemed unacceptable. Therefore a synchronous rectifier, the basic circuit of which is shown in Figure 7 (a) was used. Here, the four diodes of the conventional bridge circuit are replaced by MOSFET switches Q1, Q2, Q3 and Q4. U1a and U1b are comparators which control the switching of the four MOSFETs when zero crossings of the a.c. input waveform are detected, switching on Q1 and Q4 for one half of the a.c. cycle and Q2 and Q3 for the other halfcycle, thus mimicking the action of a diode bridge when feeding a resistive load. The advantage gained by using MOSFET switches is that there is no forward threshold voltage to be overcome before conduction commences as with a diode, allowing the voltage lost across the rectifier to be of the order of millivolts instead of hundred of millivolts.

3.2. Control laws

Since we have the capability of providing varying damping forces by using the resistance emulator, we can design control laws to improve the performance of the TMD/H. We might also use this capability to retune the device if the external forcing or host structure suffer any modification. In this work we focus on optimising the displacement reduction of the host structure and the power available to harvest is estimated post optimization to ensure a minimum is produced to power our sensors and control law. Two low power consumption control laws were considered, the first one is an adaptive control law the second one is a semi-active control law. Both schemes are suitable

DOI: 10.1002/stc

for systems subjected to variable frequency sinusoidal loads. In this work we define an adaptive scheme as one where exchange of information and control happens over several periods of forcing and is aimed at retuning problems. In a semi-active scheme exchange of information will occur several times in within one period of forcing. To date little work has been published concerning the power usage of active or semi-active control laws, since the optimisation normally is exclusively on performance. Scruggs and Iwan [29] presented one of the first studies were the power available for the control is limited. **More recently, power-flow constrains were studied by Cassidy and Scruggs in [30]. Optimal control for maximisation of power generation is studied in [31, 32] in the presence of nonlinearities and stationary stochastic disturbances respectively.** Wang and Inman [33] summarise a comparison of four of the most widely used control laws in both terms of performance and power. **The power flow in a set of experiments is studied by [13, 34], in the context of simultaneous vibration absorption and harvesting.**
All the simulations presented in this section are run with the parameters of our experimental rig that will be presented in next section.

Adaptive control law.

We consider the definition of a frequency dependant load R_L. If the displacement of the host structure, x_p, is plotted against R_L, we obtain the results depicted in Figure 8. Two different behaviours were encountered, depending on the forcing frequency. We define ω_i as a forcing frequency such that $\omega_a < \omega_i < \omega_b$, where ω_a and ω_b are the fixed points defined by Den Hartog [2]. These fixed point frequencies are a function of μ and β and are the roots of the following equation,

$$(2+\mu)\omega_{ab}^4 - 2(1+\mu)\omega_{ab}^2 + 2\beta^2 = 0 \tag{9}$$

Correspondingly ω_{ii} is defined as a forcing frequency such that $\omega_{ii} < \omega_a$ or $< \omega_{ii} > \omega_b$.

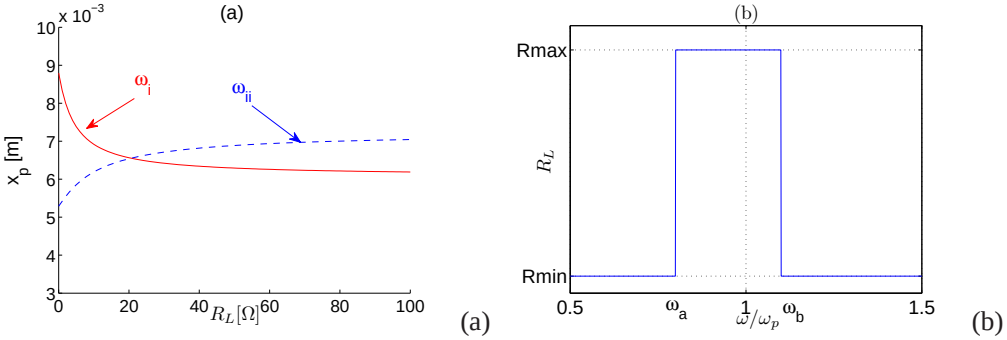

Figure 8. (a) Host structure displacement versus resistive load (b) Adaptive control law

As it can seen in the Figure 8, for excitation frequencies between ω_a and ω_b (ω_i), displacement x_p tend to a minimum as $R_L \to \infty$, on the other hand, for excitation frequencies ω_{ii}, the displacement x_p is minimum for $R_L = 0$. These correspond to open and short circuit respectively. Since in both cases no power will be available to harvest, suboptimal values (from an suppression point of view) $R_L = R_{min}$ and $R_L = R_{max}$ corresponding to acceptable levels of power, will be used. We defined acceptable level of power as the minimum necessary to power a number of complex sensor nodes, including at least a wireless sensor and a microprocessor. For this set of simulations a minimum a 50mW is used. This amount would allow common low power wireless protocols or even power a MP3 player [35]. See Casciati and Rossi [36] for more information on optimising a wireless control unit to use in a structural control scenario. This power, $50mW$, has to be produced when the host structure displacement exceeds an onset value to be defined. Combining the host structure displacement with the power available to harvest versus R_L curves for the isolated harvester [25],

DOI: 10.1002/stc

the two values R_{min} and R_{max} can be estimated. The suboptimal adaptive control law is shown in Figure 8 (b).

Figures 9 and 10 show numerical simulations, comparing passive and adaptive devices. The host structure is defined by $\mu = 0.2$, $\beta = 1/(1+\mu)$ and $\zeta_p = 0.02$. Where x_{po} is the displacement of the host structure without any absorbing device, x_p is the host structure displacement when a passive TMD/H is connected, x_{pca} is the displacement of the host structure when using the adaptive control law and x_s is the displacement of the TMD/H. The lower R_{min} and the higher R_{max} the more we can reduce the displacement of the host structure. In this set of simulations $R_{max} = 100\Omega$ and $R_{min} = 3\Omega$ so a minimum of 50mW is available to harvest, see Figure 9 (c). Due to the existence of the fixed points, with this strategy the adaptive device can not improve the performance of a passive device for excitation frequencies equal to ω_a or ω_b.

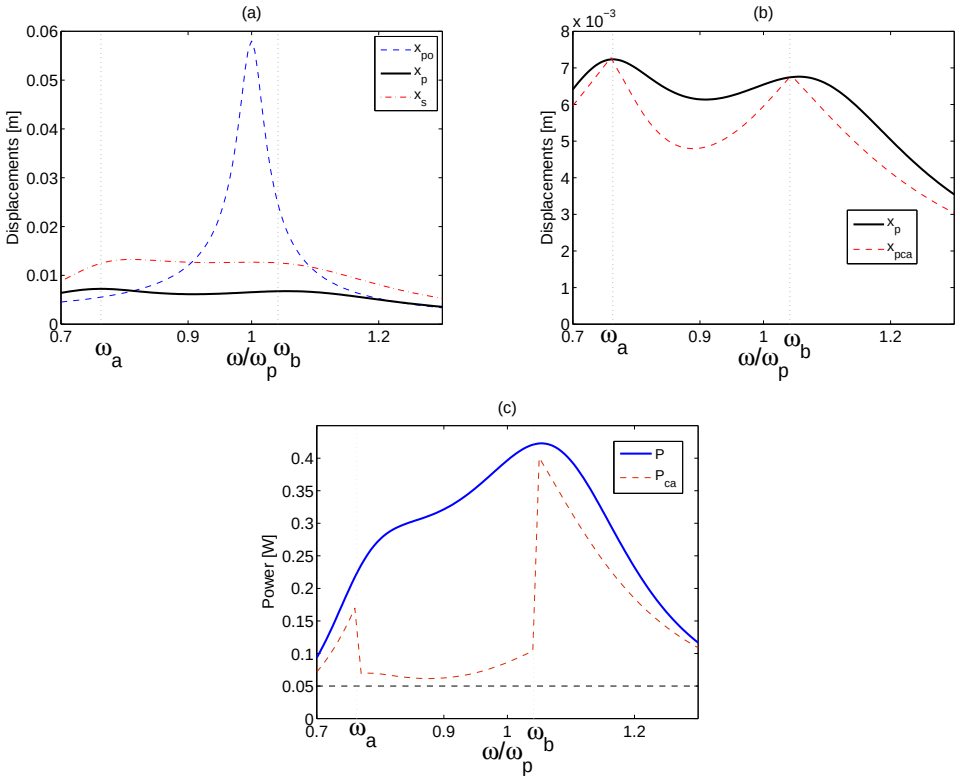

Figure 9. Numerical simulations comparing passive versus adaptive device.(a) Host structure displacement before x_{po} and after x_p installing a passive TMD/H. (b) Host structure displacement comparison between a passive device x_p and an adaptive one x_{pca}. (c) Power available to harvest using a passive when using a passive device P and an adaptive one P_{ca}

We note that a possible strategy to overcome this limitation might be to connect in series with the resistance emulator and impedance that will change the apparent stiffness or apparent mass of the TMD/H. Three branches might be connected in parallel, governed by three switches. The first one with R_L, the second with a capacitor to increase the apparent mass of the TMD/Harvester , the third one with an inductance to increase the apparent stiffness of the TMD/Harvester, see Figure 10(a). In Figure 10(b) shows example results from a simulation of such scheme where the apparent stiffness and mass are changed by 5% such that $M_{s2} = 1.05M_s$ if $\omega < 1.02\omega_a$ and $K_{s2} = 1.05K_s$ if $\omega > 0.98\omega_b$. However, this is not fully explored here, we note a discussion on using a generic impedance to address tuning can be found in [24].

For the experiments described in section 4, the adaptive control law operates as follows. The frequency of the response (and therefore excitation) is monitored by timing the induced voltage

DOI: 10.1002/stc

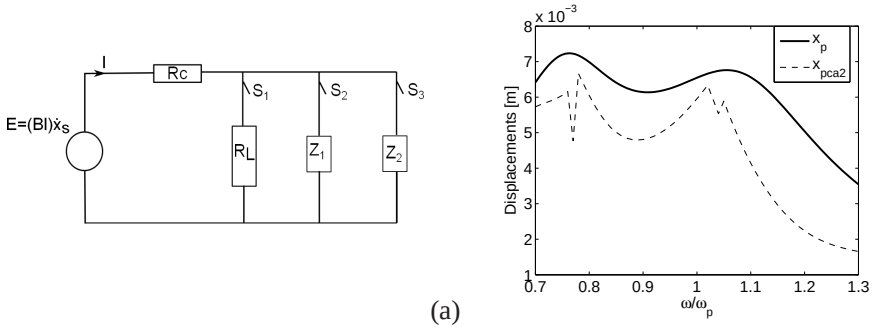

Figure 10. (a) Proposed circuit to overcome the fixed points limitation. (b) Numerical simulation results for the second adaptive control law.

zero crossings,which occur a t_{ci}, $\omega = \dfrac{2\pi}{t_{cn} - t_{c(n-1)}}$, this frequency is compared with ω_a and ω_b, optimal R_L is extracted from law shown in Figure 8 and the appropriate control voltage is sent to the resistance emulator. Exchange of information occurred every minute.
$Semi - active\ control\ law.$

We now consider a base-excited system, a typical scenario for earthquake engineering or vehicle suspension problems, as defined in Figure 1(b), where the objective is to minimize the relative displacement of the host structure. We follow a Ground Hook control methodology [37], with some variations to accommodate physical limitations and power level requirements. The Ground Hook control methodology relies on a variable damping force, in our case F_{EM}, being changed between low and high states. The two more common types of this semi-active damper are on-off (or bang-bang) and continuous ground hook strategies. Continuous GHTMD optimization is studied in [37], where it was concluded that it can outperform a passive TMD by 10% when $\zeta_p = 0.01$ (with the performance being measured as the ratio between maximum responses). The lower the damping in the host structure, ζ_p, the better continuous GHTMD will perform, with a maximum improvement of around20%.
Taking into account dissipative damping, power requirements and values covered by the resistance emulator, the following continuous Ground Hook control law is defined,

$$C_T = \begin{cases} \dot{x}_p(\dot{x}_p - \dot{x}_s) \geq 0 \begin{cases} G\dfrac{\dot{x}_p}{\dot{x}_p - \dot{x}_s} \geq C_{min} \rightarrow min\left\{G\dfrac{\dot{x}_p}{\dot{x}_p - \dot{x}_s}, C_{max}\right\} \\ otherwise \rightarrow C_{min} \end{cases} \\ otherwise \rightarrow C_{min} \end{cases} \tag{10}$$

where G relates damping level C_T to $\dot{x}_p$. In the present study the values for C_{min} and C_{max} will be conditioned by: the amount of mechanical damping, the minimum power that we require to harvest and the R_L range of values the resistance emulator is able to cover. Keeping C_{min} and C_{max} within achievable values, we will show that the parameters G and β, can be optimised such that the GHTMD can outperform a passive TMD.
In order to simplify the controller a bang-bang strategy can be used. **In optimal control theory a control function is bang-bang if it uses only extreme points of the constraint set. For a linear differentiable system any attainable state can also be reached by using a bang-bang control, [38].** We propose the following bang-bang Ground Hook Control law:

$$C_T = \begin{cases} \dot{x}_p(\dot{x}_p - \dot{x}_s) \geq 0 \begin{cases} K_G \dfrac{\dot{x}_p}{\dot{x}_p - \dot{x}_s} \geq C_{min} \rightarrow C_{max} \iff ON \\ otherwise \rightarrow C_{min} \iff OFF \end{cases} \\ otherwise \rightarrow C_{min} \iff OFF \end{cases} \tag{11}$$

Figure 11 show the numerical results obtained when applying the Ground Hook control laws defined by equations 10 and 11. Note that since the system is excited at its base and the objective is to minimise relative displacements, Den Hartog's formulas for optimal passive device do not hold. For base excitation, following the same strategy proposed in [2], the optimal frequency ratio is found to be $\beta = \sqrt{\dfrac{2-\mu}{2(1+\mu)^2}}$, the optimal total damping ratio was found numerically to be $\zeta_T = 0.26$. Figure 11 (a) show the numerical results for a passive optimised TMD, a continuous Ground Hook TMD/H and three bang bang Ground Hook TMD/H. It can be seen that by adjusting C_{max} and K_G, the bang bang Ground Hook controller performance is comparable to the continuous Ground Hook one, see (v) and (ii) in Figure 11 (a) . Using the same performance index defined in [37], and comparing a passive TMD with the bang bang Ground Hook TMD/H we obtain an improvement of 8%. Table II summarises the values for this simulation.

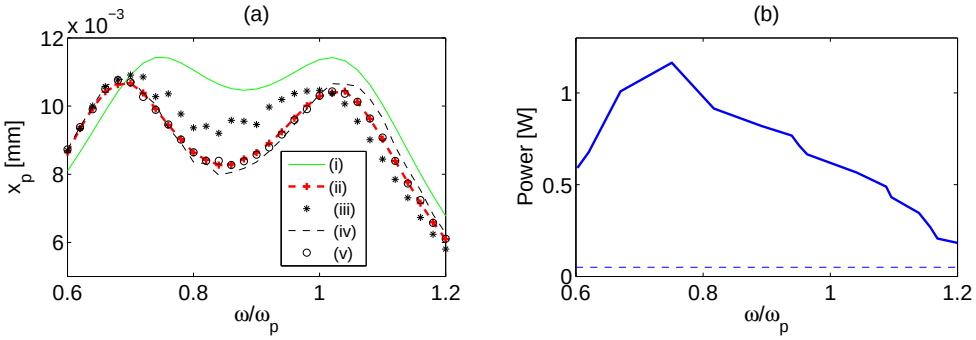

Figure 11. Numerical simulations, (a) Host structure displacement, passive TMD, continuous and bang bang GHTMD/H, (b) Average power available to harvest for simulation (v).

Simulation	C_{min}	C_{max}	β	$Swicthing$
(i) Passive	n/a	n/a	0.79	n/a
(ii) Continuous	23	65	0.74	G=65
(iii) BBGH	23	65	0.74	K_G=65
(vi) BBGH	23	70	0.74	K_G=30
(v) BBGH	23	60	0.74	K_G=40

Table II. Parameters using for simulation in Figure 11 All simulations $\mu = 0.2$

For the experiments described in section 4, the semi active control law operates as follows. The relative displacement of the host structure x_p, see Figure 1 (b), is monitored and compared to the relative displacement of the TMD/H $x_s - x_p$. The appropriate voltage is sent to the resistance emulator following the control law described in Equation 11. Exchange of information occurred every millisecond.

DOI: 10.1002/stc

4. EXPERIMENTAL VALIDATION

The system represented by Figure 1 is studied experimentally using Real Time Dynamic Substructuring Testing [21, 39]. The system is divided into two subsystems: a numerical one and a physical one. The host structure is the numerical substructure which is simulated in the computer while the TMD/H is physically built. Both subsystems interact in real time while running the tests, following the substructuring loop depicted in Figure 12 , corresponding to a forced host structure. To implement the real-time tasks a dSpace DS1104 RD controller board was used in conjunction with a MATLAB/ Simulink model as shown in Figure 12. The displacement output from the numerical model was computed using a fourth-order Runge Kutta-type explicit integration scheme. The dSpace module ControlDesk is used for on-line analysis and control. All these elements together provide one integrated tool to manage the real-time substructuring experiments. The transfer system consists of an electrically driven ball-screw actuator with an in-line synchronous servo-motor controlled by a servo-drive which applies a displacement to the TMD/H base, Figure 12 shows a photograph of the experimental apparatus. The instrumentation used consists of an accelerometer measuring absolute acceleration of the TMD/H mass and 2 LVDTs displacement transducers, measuring absolute displacement of the base of the harvester and relative displacement between harvester and its base.

The experiments were run with a $1ms$ sampling time. The delay introduced by the actuator transfer system was measured at $18ms$ and compensated by a polynomial fitting prediction technique, as described in [21]. The feedback force is measured via an accelerometer connected to the shaft moving mass, measuring the absolute acceleration $\ddot{x}_s + \ddot{x}_p$ and taking into account that $f_s = M_s(\ddot{x}_s + \ddot{x}_p)$. Rearranging equation 1 we obtain

$$M_p\ddot{x}_p + C_p\dot{x}_p = f_e - (K_p x_p - C_s\dot{x}_s - K_s x_s - F_{EM}) = f_e - M_s(\ddot{x}_p + \ddot{x}_s) = f_e - f_s \tag{12}$$

At each time step the displacement of the base of the harvester (i.e displacement of the host structure due to the forcing) is calculated numerically from external excitation F_e and measured substructuring force F_s. The displacement is applied to the experimental subsystem, the TMD/H and the force F_s is measured and fed back to calculate next time step. The cycle is repeated until the end of the test.

In this set of experiments we set our power target at $50mW$, as in the previous simulations. Note a complex sensor node includes microprocessor and its power demand can be estimated at $100\mu W$ although this is very sensitive to each different application [35]. It is important to note that in full size applications the levels of power available to harvest will be considerable higher that the ones presented in this paper, in the order of tens or hundreds of watts [14]. Due to high levels of parasitic damping in our voice coil transducer, we are limited in our test to relatively high values of μ, namely $\mu = 0.2$.

4.1. Adaptive control law experimental results

For this sets of experiments, we use $\mu = 0.2$, $\beta = 1/(1+\mu)$ and $\zeta_p = 0.02$. Following the control law defined by Figure 8, and using $R_{min} = 7\Omega$ and $R_{max} = 100\Omega$ we obtain the experimental results are gathered in Figure 13. A passive device was also tested by setting an optimal $R_L = 21\Omega$. A reduction of the primary system response between 3-15$\%$ is achieved by using the adaptive control law instead of a passive device, the minimum reduction corresponding to the neighbourhood of the fixed points. The harvested power when using the adaptive scheme is above the $50mW$ limit for all tested frequencies.

Semi active TMD/H

We study now the system represented in Figure 1 (b), were the host structure is subjected to ground acceleration. $\zeta_p = 0.01$ for this set of experiments. Due to the ground motion the substructruring loop differs slightly from the one represented in Figure 12. The new equations of motion, in terms

DOI: 10.1002/stc

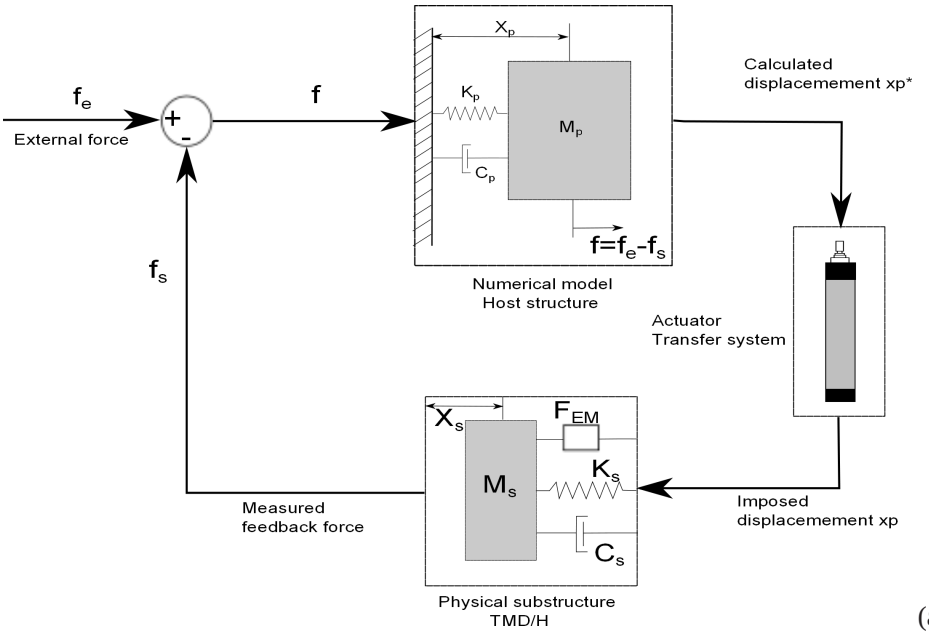

(a)

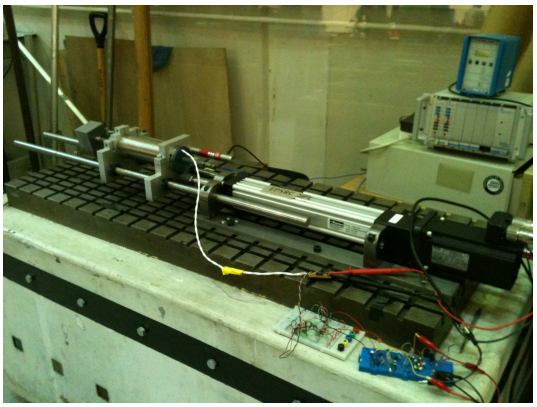

(b)

Figure 12. Substructuring loop for a forced host structure (a) and experimental rig set-up (b). f_e external forcing, f_s measured feedback force, x_p^* displacement calculated by the numerical model and sent to the transfer system and x_p displacement applied by the transfer system to the TMD/H

of relative displacements to the ground, can be written as:

$$\begin{aligned} M_p\ddot{x}_p + C_p\dot{x}_p + K_p x_p - C_s(\dot{x}_s - \dot{x}_p) - K_s(x_s - x_p) - F_{EM} = -M_s a_g \\ M_s(\ddot{x}_s + ag) + C_s(\dot{x}_s - \dot{x}_p) + K_s(x_s - \dot{x}_p) + F_{EM} = 0 \end{aligned} \tag{13}$$

where a_g is the ground motion acceleration. Therefore the dynamics of the numerical model can be written as,

$$M_p\ddot{x}_p + C_p\dot{x}_p + K_p x_p = -M_s a_g - M_s(\ddot{x}_s + ag) \tag{14}$$

The absolute displacement of the host structure will be applied to the base of the TMD/H and the substructuring force $M_s(\ddot{x}_s + a_g)$ will be fed back to the numerical model to solve equation 14.

The first step to optimise the semiactive TMD/H is to estimate the parameters C_{max} and C_{min} that can be achieved by the TMD/H. Our resistance emulator is able to cover a range from 4Ω to 325Ω, see figure 7. Taking into account that $C_T = C_{mec} + \dfrac{(BL)^2}{R_c + R_L}$ we obtain $C_{min} = 21.4N/(m/s)$ and

DOI: 10.1002/stc

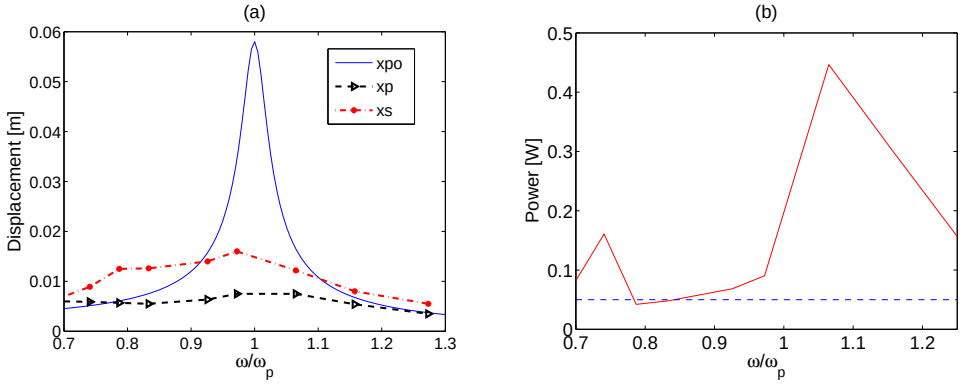

Figure 13. Experimental results, (a) Host structure displacement before x_{po} and after x_p coupling TMD/H and TMD/H displacements x_s (b) Power available to harvest by the TMD/H.

$C_{max} = 39.5N/(m/s)$. Secondly the frequency ratio β has to be optimised, so the two maximum points of the curve x_p versus r, are as the same level. We start by applying a ON/OFF control low where $K_G \to \infty$, i.e.

$$C_T = C_{max} \text{ if } 0 \leq \frac{\dot{x}_p}{(\dot{x}_p - \dot{x}_s)} \qquad C_T = C_{min} \text{ otherwise} \tag{15}$$

the value of K_G will be adjusted in a final step.

The results from the second optimization step are presented in Figure 14, the ratio β is changed from one experiment to another by changing the numerical K_p while maintaining the values of μ and ζ_p. The forcing level is kept at $a_g = 1.5m/s^2$. The optimal β was found to be approximately 0.87. Once optimal β has been estimated, K_G is varied to obtain an optimal value, in this case it was found to be $K_G = 5 \times 10^4$.

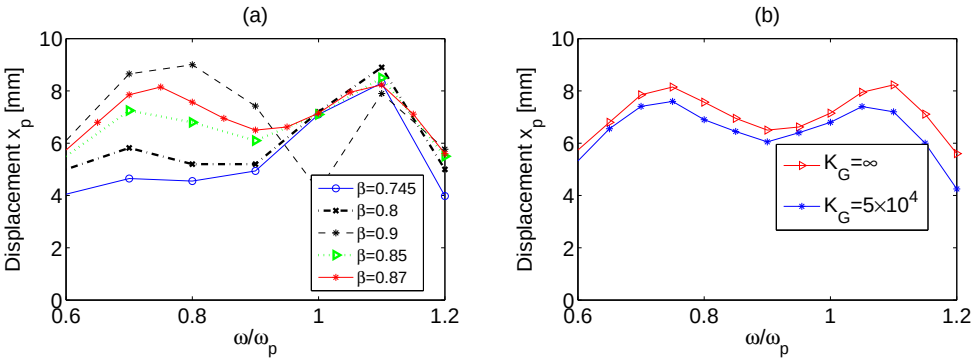

Figure 14. Experimental semi-active controller optimisation. (a) Finding the optimal β (b) After β is fixed, finding optimal K_G.

The results using these optimal values of β and K_G with $\mu = 0.2$ and $a_g = 1.8m/s^2$ are shown in Figure 15.Figure 15 (a) show the reduction of the displacement of the Host structure x_p before and after TMD/H coupling, (b) shows the measured power available to harvest which is above 50mW for all tested frequencies.

DOI: 10.1002/stc

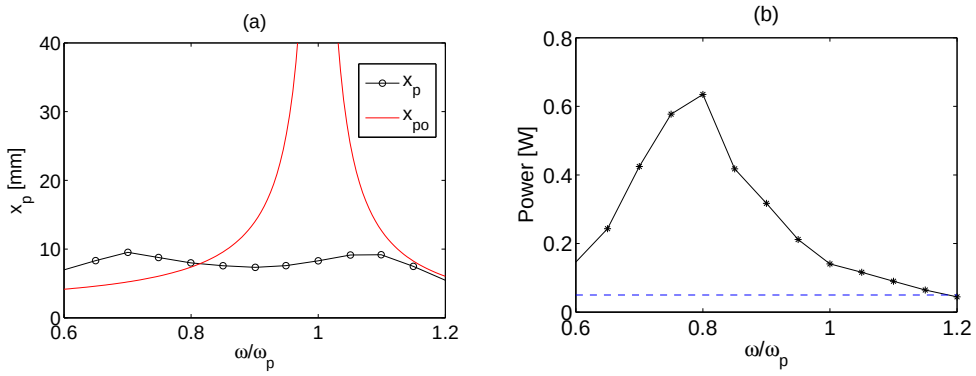

Figure 15. Experimental results using a semi-active controller. (a) Displacement of the host structure before x_{po} and after x_p installing the TMD/H and (b) Power available to harvest by the TMD/H.

CONCLUSIONS

This paper presents both analytical and experimental results from a tuned mass damper/harvester, capable of reducing the response of a host structure and harvesting power to be used by the control algorithm. Two low power control laws were presented and applied experimentally. The performance in terms of host structure displacement shows an improvement from a passive device. Moreover the levels of power harvested suggest there is no need of external power for the controller and enough power to run a network of sensors to provide heath monitoring capabilities. The analytical predictions were validated experimentally: the existence of fixed points as well as the performance dependence on R_L were experimentally found, with small deviations from the mathematical model due to non-linearities non included in the model. As anticipated numerically, the semi-active controller shows a better performance than the adaptive controller in both terms of host structure displacement and power available to harvest. With the semi active controller the performance was improved by 8%, with the adaptive one by 3%, both of them harvesting above $50mW$ across the frequency range of interest. Both vibration absorption and energy harvesting will be enhanced if a device with lower parasitic damping and lower coil resistance is used. From the vibration absorption point of view, low parasitic damping gives more flexibility in the choice of mass ratio values μ. High values of parasitic damping will limit the application of this technique to higher values of μ. The less parasitic damping, the less energy is lost in a dissipative way and the more energy will be available to harvest. The development of such systems, low parasitic damping and low R_c, will be the aim of future work together with the creation of synthetic impedance allowing not only damping regulation but frequency tuning in real time.

ACKNOWLEDGEMENTS

AGB and AC are supported by EPSRC grant EP/J008532/1. SAN is supported by an EPSRC fellowship grant EP/K005375/1. SGB is supported by a RAEng Leverhulme Trust Senior Research Fellowship.

REFERENCES

1. H. Frahm. Device for damping vibrations of bodies. Patent No. 989, 598, 1911.
2. J.P. Den Hartog. *Mechanical Vibrations*. New York: McGraw-Hill, 1947.
3. F. Giuliano. Note on the paper Optimum parameters of tuned liquid columngas damper for mitigation of seismic-induced vibrations of offshore jacket platforms by Seyed Amin Mousavi, Khosrow Bargi, and Seyed Mehdi Zahrai. *Structural Control and Health Monitoring*, 20:852, 2013.

DOI: 10.1002/stc

4. S. Casciati and F. Giuliano. Performance of Multi-TMD in the Towers of Suspension Bridges. *Journal of Vibration and Control*, 18:821–847, 2009.
5. D. Hovrat, P. Barak, and M. Rabins. Semi-active versus passive or active tuned mass dampers for structural control. *Journal of Engineering Mechanics*, 109(3):691–705, 1983.
6. T. T. Soong and G. F. Dargush. *Passive Energy Dissipation systems in Structural Engineering*. John Wiley and Sons, 1997.
7. B. F. Spencer and S. Nagarajaiah. State of the art of structural control. *Journal of Structural Engineering*, 129(7):845–856, 2003.
8. T. Kobori. Towards a common goal via different road. *Structural Control and Health Monitoring*, 13(1):7–9, 2006.
9. F. Casciati, J. Rodellar, and U. Yildirim. Active and semi-active control of structures - theory and applications: A review of recent advances. *Journal of Intelligent Material Systems and Structures*, 23(11):1181–1195, 2012.
10. S. Nagarajaiah. Adaptive passive, semiactive, smart tuned mass dampers: identification and control using empirical mode decomposition, hilbert transform, and short-term fourier transform. *Structural Control and Health Monitoring*, 16:800–841, 2009.
11. S. Priya and D. J. Inman. *Energy Harvesting Technologies*. Springer, 2009.
12. S. Adhikari and F. Ali. Energy harvesting dynamic vibration absorbers. *Journal of Applied Mechanicss*, 80(4):041004, 2012.
13. X. Tang and L. Zuo. Simultaneous energy harvesting and vibration control of structures with tuned mass dampers. *Journal of Intelligent Materials and Structures*, 23(18):2117–2127, 2012.
14. I. L. Cassidy, J. T. Scruggs, S. Behrens, and H. P. Gavin. Design and experimental characterization of an electromagnetic transducer for large-scale vibratory energy harvesting applications. *Journal of Intelligent Materials and Structures*, 22(17):2009–2011, 2011.
15. S. Zhu, W. Shen, and Y. Xu. Linear electromagnetic devices for vibration damping and energy harvesting: Modeling and testing. *Engineering Structures*, 34:198–212, 2012.
16. R. Palomera-Arias, J. J. Connor JJ, and J. A. Oschendorf. Feasibility study of passive electromagnetic damping systems. *Journal of Structural Engineering*, 134:164–170, 2008.
17. F. Casciati and R. Rossi. A power harvester for wireless sensing applications. *Structural Control and Health Monitoring*, 14:649–659, 2007.
18. D. Mammosser, E. Foltete and M. Collet. Optimization of the power flow extracted from a flexible structure using a control approach. *Structural Control and Health Monitoring*, 18:361–381, 2011.
19. L. Zuo and P. S. Zhang. Energy Harvesting, Ride, Comfort, and Road Handling of Regenerative Vehicle Suspensions. *Journal of Vibration and Acoustics*, 135:011002, 2013.
20. S. G. Burrow and L. R. Clare. Open-loop power conditioning for vibration energy harvesters. *Electronics letters*, 45(19):999–1000, 2009.
21. A. Gonzalez-Buelga, D. J. Wagg, and S. A. Neild. Parametric variation of a coupled pendulum-oscillator system using real-time dynamic substructuring. *Structural Control and Health Monitoring*, 14(7):991–1012, 2007.
22. J. M. Londono, G. Serino, D. J. Wagg, S. A. Neild, D. J. Crew. On the assessment of passive devices for structural control via real-time dynamic substructuring. *Structural Control and Health Monitoring*, 19:701–722, 2012.
23. N. G. Stephen. On energy harvesting from ambient vibration. *Journal of Sound and Vibration*, 293:409–425, 2006.
24. A. Cammarano, S. G. Burrow, D. A. W. Barton, A. Carrella, and L. R. Clare. Tuning a resonant energy harvester using a generalized electrical load. *Smart Material and Structures*, 19(055003), 2010.
25. L. R. Clare and S. G. Burrow. Power conditioning for energy harvesting. Proccedings of the SPIE. Ahmadian, Mehdi., 2008.
26. A. Kasyap, J. S. Lim, D. Johnson, S. Horowitz, T. Nishida, K. Ngo, M. Sheplak and L. Cattafesta. Energy reclamation from a vibrating piezoceramic composite beam. Proccedings of the Ninth International Congress on Sound and Vibration, ICSV9 2002.
27. G. K. Ottman, H. F. Hofmann and G. A. Lesieutre. Optimized Piezoelectric Energy Harvesting Circuit Using Step-Down Converter in Discontinuous Conduction Mode. *IEEE Transactions on Power Electronics*, 18:696–703, 2003.
28. E. Lefeuvre, D. Audigier, C. Richard and D. Guyomar. Buck-Boost Converter for Sensorless Power Optimization of Piezoelectric Energy Harvester. *IEEE Transactions on Power Electronics*, 22:2018–2025, 2007.
29. J. T. Scruggs and W. D. Iwan. Structural control with regenerative force actuation networks. *Structural Control and Health Monitoring*, 12:25–45, 2005.
30. I. L. Cassidy and J. T. Scruggs. Nonlinear stochastic controllers for power-flow-constrained vibratory energy harvesters. *Journal of Sound and Vibration*, 332:3134–3147, 2013.
31. I. L. Cassidy and J. T. Scruggs. Statistically linearized optimal control of an electromagnetic vibratory energy harvester. *Smart Materials and Structures*, 21:085003, 2012.
32. J. T. Scruggs , I. L. Cassidy and S. Behrens. Multi-objective optimal control of vibratory energy harvesting systems. *Journal of Intelligent Material Systems and Structures*, 23(18):2077–2093, 2012.
33. Y. Wang and D. J. Inman. Comparison of control laws for vibration suppression based on energy consumption. *Journal of Intelligent Material Systems and Structures*, 22:795–809, 2011.
34. X. Tang and L. Zuo. Simulation and Experiment Validation of Simultaneous Vibration Control and Energy Harvesting from Buildings using Tuned Mass Dampers. *American Control Conference*, 2011.
35. R. J. M. Vullers, R. van Schaijk, I. Doms, C. Van Hoof, and R. Mertens. Micropower energy harvesting. *Solid-State Electronics*, 53:684–693, 2009.
36. S. Casciati and Z. Chen. A multi-channel wireless connection system for structural health monitoring applications. *Structural Control and Health Monitoring*, 18:588–600, 2011.
37. M. Setareh. Application of semi-active tuned mass dampers to base-excited systems. *Earthquake Engineering and Structural Dynamics*, 30:449–462, 2001.
38. Z. Artstein. Discrete and continuous bang-bang and facial spaces or: look for the extreme points. *SIAM J. Review*, 22:172–185, 1980.

39. A. Blakeborough, M. S. Williams, A. P. Darby, and D. M. Williams. The development of real-time substructure testing. *Philosopical Transactions of the Royal Society of London A*, 359:1869–1891, 2001.

DOI: 10.1002/stc